RSC Advances

ROYAL SOCIETY OF CHEMISTRY

www.rsc.org/advances

Flexible cellulose acetate/graphene blueprints for vibrotactile actuator

Md Mohiuddin, Kishor Kumar Sadasivuni, Seongcheol Mun, Jaehwan Kim*

Center for EAPap Actuator, Dept. of Mechanical Engineering, Inha University, 253 Yonghyun-Dong, Nam-Ku, Incheon 402-751, South Korea

Corresponding Author

Tel.: +82 32 860 7326; Fax: +82 32 832 7325

E-mail: jaehwan@inha.ac.kr (Jaehwan Kim)

Abstract

Tactile devices containing many actuators within are being sutured using electroactive polymers. This innovation forms the basis of hand-like-tactile feedback in the emerging smart robotic manipulation. Here we introduce low power consuming modified reduced graphene oxide embedded cellulose acetate composite of high flexibility and conformability to surfaces made by simple and low cost synthesis methods and thus points towards simple read-out electronics. The material performance was evaluated based on various actuation conditions in terms of electrical potential, bias voltage, temperature and frequency. The actuator vibrating at various frequencies with faster response time illustrates a range of haptic feedbacks to users which can be used in braille display devices. Excellent repeatability of haptic actuation process was also noticed.

Keywords: Eco-friendly, Vibrotactile, Cellulose, Graphene, Braille Display

1. Introduction

The interdisciplinary research fields like bio-inspired robotics, sensors, biomedical devices, touch-feedback haptic systems, flexible soft electronics etc. exploit polymer based actuators driven by electrical stimuli to design and control virtual reality.[1] The word haptics refers to any form of nonverbal communication involving the application of a touch response in a user interface design to provide information to an end user. Very recently the haptics research has gained much importance as more physical and realistic virtual experience is created by the actuators embedded in the device. The tactile-feedback technology developed in mobile electronic devices provides touch sensation along with visual and auditory recognition and thus more realistic user experiences.[2–4] Such feedback devices using electrostatic force are also considered to be promising for touch based electronics.[5, 6] Developing a full page refreshable braille tactile sensing display needs many small diameter actuators with higher energy density to move the pins.[7, 8] The actuators present in the commercially available displays require a significantly larger area than the braille pins themselves and so the displays are bulky, expensive and limited to two lines of braille characters. In this regard designing a more compact and portable system capable of identifying the symbols and interfacing the blind community freely with computers has utmost importance.

Many kinds of braille displays used right now possess contractible multilayer stacked actuators,[9] bistable electroactive polymers that use temperature control,[10] dielectric buckling elastomer membranes[11, 12] and polyvinylidene fluoride (PVDF) bending bimorph actuators coupled with hydraulic fluids.[13] It is very necessary to build up eco-friendly tactile sensors of high flexibility and sensitivity at low-range voltage to apply in braille displays. Piezoceramic actuators are capable of producing vibrations at a wide frequency range from a small device,[14–16]

but with difficulty in selectively stimulating mechanoreceptors as their vibrations are not enough except at their resonance frequencies. Instead of such materials, PVDF and copolymers have been studied for fabricating tactile sensors and actuators.[17, 18] However their melting nature and less availability promoted the invention of smart cellulose derivatives of light weight, eco-friendliness, low price, thermal stability, biocompatibility and biodegradability, very recently.[12,19-22] The cellulose acetate (CA) possesses potential compatibility, excellent optical and mechanical properties and good dielectric constant and is used to manufacture fibers, films, laminates, adhesives, coatings, plastic products and tactile actuators.[1, 23, 24] The electrically active nano-additives, such as carbon nanotubes (CNTs) and graphene improve the mechanical properties of CA and enable the multi-functionality needed for electrical energy storage, sensing, and actuation.[1, 19, 25-28] Out of various nanocarbon additives, graphene is the most investigated due to its excellent electrical properties, mechanical strength, and flexibility.[29-32] The transistors, solar cells, sensors, batteries and supercapacitors based on flexible graphene renders it suitable for a wide range of flexible electronic devices.[12, 33, 34] The outstanding capability of such materials to convert physical contacts into electric signals allows it to be utilized in high-performance flexible tactile sensors.[32, 35, 36]

In this paper, we present a new rolled CA/graphene composite that meets all of vibrotactile actuator specifications with low voltage operation based on electrostatic potential. The fabrication process, performance evaluation and electrostatic behavior of this haptic actuator are discussed here on the basis of modification of the reduced graphene oxide (RGO) and the concentration of modified reduced graphene oxide (m-RGO). We analyze the morphologies, electrical and optical properties of CA/graphene composite by scanning electron microscopy

(SEM), X-ray diffraction (XRD), semiconductor device analyzer and UV-visible spectrophotometer technologies as well.

2. Experimental Section

Materials

Cellulose acetate powder ($C_{76}H_{114}O_{49}$), triethyl citrate (TEC, $C_{12}H_{20}O_7$), natural flake graphite, and other reagents such as hexamethylene-1,6-diisocyanate (HMDI), dimethyl acetamide (DMAc), lithium chloride (LiCl), sulfuric acid (H_2SO_4), nitric acid (HNO_3), hydrochloric acid (HCl), Potassium permanganate ($KMnO_4$) and 30% hydrogen peroxide (H_2O_2) solution were procured from Sigma-Aldrich. The 99.5% isopropyl alcohol and acetone were purchased from Daejung, South Korea.

Synthesis of m-RGO

The synthesis of GO was carried out by oxidizing graphite followed by the improved graphene oxide synthesis method.[37] The synthesized graphene oxide had a flake thickness of ~1.5nm and width about ~1.5μm as shown in Figure S2. The modification for RGOs was done by dissolving the required amounts of GO and HMDI in DMF and sonicating for 10 min. The mixture was then refluxed for 48 h at 100 ^{o}C. The precipitate was filtered and washed several times with DMF to remove the extra methyl isocyanate.[21, 38] The product was dried in a vacuum oven at 60^{o}C to obtain the functionalized GO nanosheets methyl isocyanate complex.

Preparation of CA/m-RGO composite

The CA was dissolved in acetone at 7.5% (7.5:92.5) and mechanically stirred for about 3 hours at room temperature. Followed by this, TEC (plasticizer material) and homogeneous dispersions of 1 wt% m-RGO are dissolved one after the other in the solvent mixture by magnetic stirring. Subsequently around 20 ml of solution was slowly poured in a silicon wafer and left in room temperature for drying. Finally a flexible and transparent composite film typically 200 μm thick was obtained. In order to investigate the effect of the m-RGO sheets on the performance of vibrotactile actuator, in addition to the CA/m-RGO composite film, a pristine CA film was also prepared. The electrodes for the study are made by spraying thin layer of silver nanowires (AgNWs) on the side of the composite film. The spacers in between two films allow the actuator to vibrate in plane perpendicular direction and the finalized samples were tested on glass substrate at an ambient condition.

Characterization

Field emission SEM images of the sample films were taken with JEOL JSM-6400F microscope to study the sample morphology. The samples were prepared by coating platinum layer using an ion sputter (EMITECH, K575X). XRD patterns were checked with a thin film X-ray diffractometer using CuKα target radiation at 40 kV and 50 mA, at a scanning rate of 0.015°/min. The diffraction angle was varied from 5 to 40°. Optical transmittance of the samples was studied using a UV-visible spectrophotometer. For this the spectra of the films in the range of 200-700 nm wavelengths were recorded with a diode array (HP, 8452A). The variation in dielectric properties of the samples during 20 Hz - 1 kHz frequency was monitored using LCR meter (HP, 4284A). Measurements were done at room temperature. Setup for vibrotactile actuator with function generator (Agilent, 33220A), high voltage amplifier (Trek, 20/20), laser Doppler vibrometer (LDV; Ometron, VS-100), data acquisition system (B&K, PULSE) and

LabVIEW software installed in a computer used to stimulate actuator and measure vibration velocity is as shown in Figure S1. An element of haptic actuator is made by using film with patterned adhesive tape spacer, and then haptic actuator elements arrayed embed in device.

3. Results and Discussion

Morphology

The morphology of the materials fabricated was observed with the help of SEM images. Figure 1 shows the SEM pictures of the surface and cross sections of the CA and CA/m-RGO composite films. The morphology of CA consists of smooth surface and cross-section whereas in the CA/graphene composite case a rough surface is seen due to large graphene flakes dispersed.

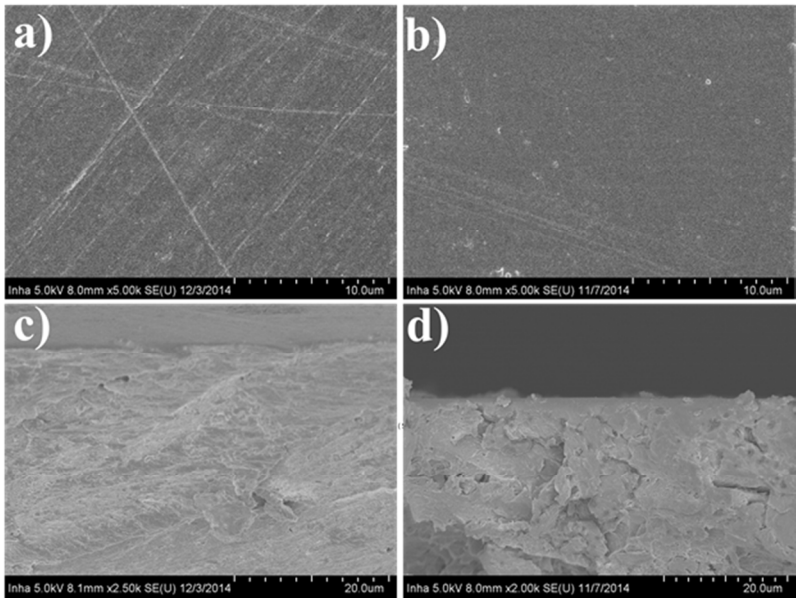

Figure 1. SEM image of CA a) surface and c) cross section; CA/m-RGO b) surface and d) cross section.

The effect of filler nanosheets on the microstructure of the CA is very lucid from the pictures shown Figure 1b and 1d. The smooth fractured surface of pristine CA becomes rough due to the presence of m-RGO (Figure 1d). Here the exfoliated m-RGO nanosheets are

uniformly dispersed in the CA medium as evidenced by the CA/m-RGO which can be attributed to the increased interaction between CA and m-RGO.

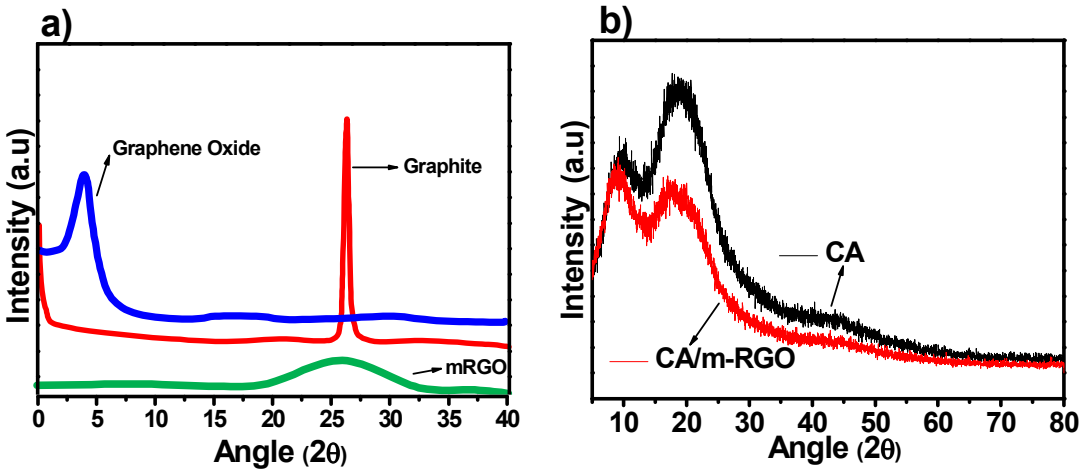

Figure 2. XRD spectra of a) graphite, GO and modified RGO and b) CA and CA/m-RGO.

To further analyze the m-RGO dispersion in the polymer, the structural variation within the filler as well as the composites was investigated through XRD studies. As shown in the XRD pattern (Figure 2a), the characteristic sharp peak of graphite at $2\theta=26.5^{o}$ is more broadened (Figure 2a) and shifted to $2\theta= 5.3^{o}$ in GO. This is due to the delamination of individual GO layers from graphite by the oxidation and sonication processes. This enhances the interlayer distance and causes a partial loss of regularity of the GO sheets. For GO, the characteristic peak is even less clear, indicating a wide range of interlayer spacing and a more substantial amount of exfoliation due to the surface modification[39]. The m-RGO, on the other hand, exhibits a peak corresponding to the d-spacing of 0.38 nm along the (002) orientation. This can be explained as the removal of oxygen functional groups causing a decrease in d-spacing. In the composite samples, the case is rather different (Figure 2b). The neat CA peak obtained near $2\theta=21^{o}$ is a crystalline halo attributed to its structure. For CA/m-RGO, the peak intensity marginally reduces

though it remains at the same position at 2θ=21°. This can be related to the crystallinity imparted to the CA matrix by the m-RGO addition. The m-RGOs possess a strong nucleating effect within the polymer matrix. In addition, the XRD spectrum of the samples shows no characteristic peak at 27 °, originating from the loss of regularity or exfoliation m-RGO in the CA, which also indicates the good dispersion of fillers in CA.

Optical Transparency

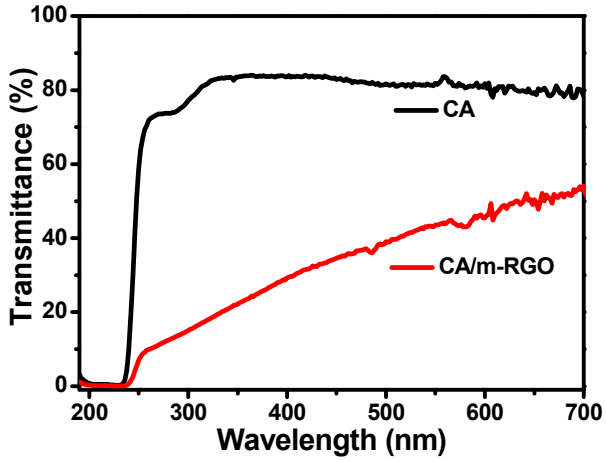

Figure 3. UV-Visible spectra of a) CA and b) CA/m-RGO.

Figure 3 presents the UV spectra of the films showing the changes in transmittance values during the wavelength, 200 to 700 nm. Generally, the graphene sheets prepared by the reduction of m-GO contain many defects in chemical and crystal structure. Combining with the layer's overlapping in the film assemblage, the optical property of composite films is inferior to pristine graphene.[29] This is because the optical transmittance of graphene-based materials is highly dependent on their defects and the number of graphene layers.[40] The transmittance was recorded well over ~80% throughout the whole visible wavelength for pristine CA film whereas

it reduced to around 40% level for m-RGO added composite film which can satisfy the requirements of certain semitransparent applications. Notably, the films possess very strong absorbance in the ultraviolet region, which would make them potential candidates for anti-UV application.

Dielectric properties

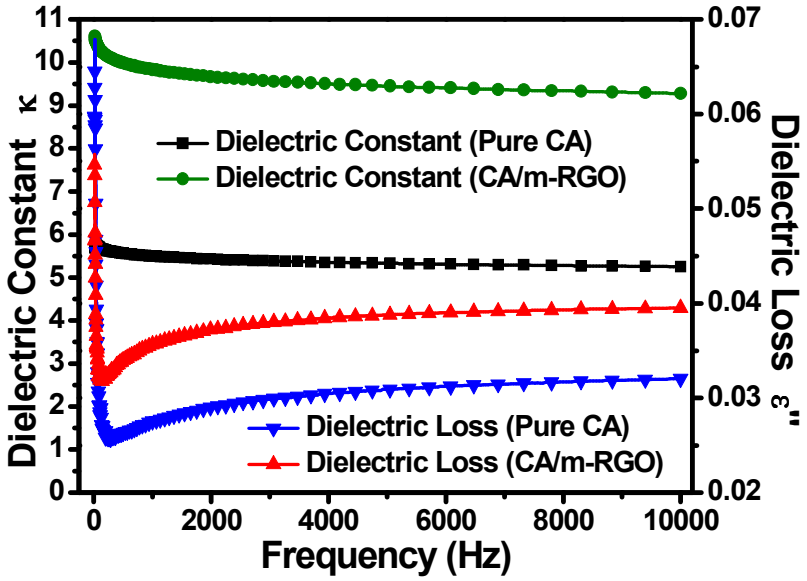

Figure 4. Variation of dielectric constant of a) CA and b) CA/m-RGO with frequency.

In order to investigate the effect of m-RGOs on the dielectric performance of CA film, frequency depended capacitance as well dielectric loss was measured by a semiconductor device analyzer over a range of frequencies, from 20 Hz to 10 kHz. Two different types of films were checked in this way, a pristine CA, and a film with the CA/m-RGO composite and the results are illustrated in Figure 4. The dielectric constant (relative permittivity) of the composite film was calculated by Equation 1,

$$\kappa = \frac{c \times d}{\varepsilon_0 \times A} \qquad (1)$$

where κ is the dielectric constant of the film, C is the capacitance, ε_0 the dielectric constant at vacuum, A and d the area of the electrode and thickness of the film, respectively.

At 150 Hz, the composite film showed a dielectric constant of 10.24 (0.032 dielectric loss) whereas the dielectric constant of CA was 5.66 with a dielectric loss of 0.027. Overall, the composite film of CA containing m-RGO exhibited around 80% increase in dielectric constant (0.037 dielectric loss) compared to the pristine CA (dielectric constant and dielectric loss were 5.54 and 0.033 respectively). Interfacial polarization at the interface between the m-RGO and the CA attribute to the increase in dielectric constant of the composite film. Upon comparing the permittivity, CA/m-RGO composite possesses enhanced values than the neat due to the motion of free charge carriers causing interfacial polarization. The enhancement in the dielectric properties can be explained by Maxwell-Wagner-Sillars process in which the polymer-filler interfacial (like donor-acceptor complexes) interaction plays the major role.[41] The charge generated from metal coated electrodes will be trapped at polymer filler interface upon applying electric field and causes ultimate improvement in the dielectric property of the composite.[42, 39]

Vibrotactile performance

The response of the composite actuators under AC excitation of 200 and 500 V and input frequency 150 Hz is shown in Figure 5 (a) and (b) respectively. The performance of the CA/m-RGO actuators increased significantly (three times higher) in comparison with those of the pure CA actuator. This is due to the contraction force produced by the electrostatic effect between the negative and positive electrodes to displace top electrode in the downward direction. When a voltage is applied to the actuator, the sample film gets charged and then generates vibration. The

motion of the actuator is concave and the actuator performance was modulated by increasing the voltage level of the electric potential.

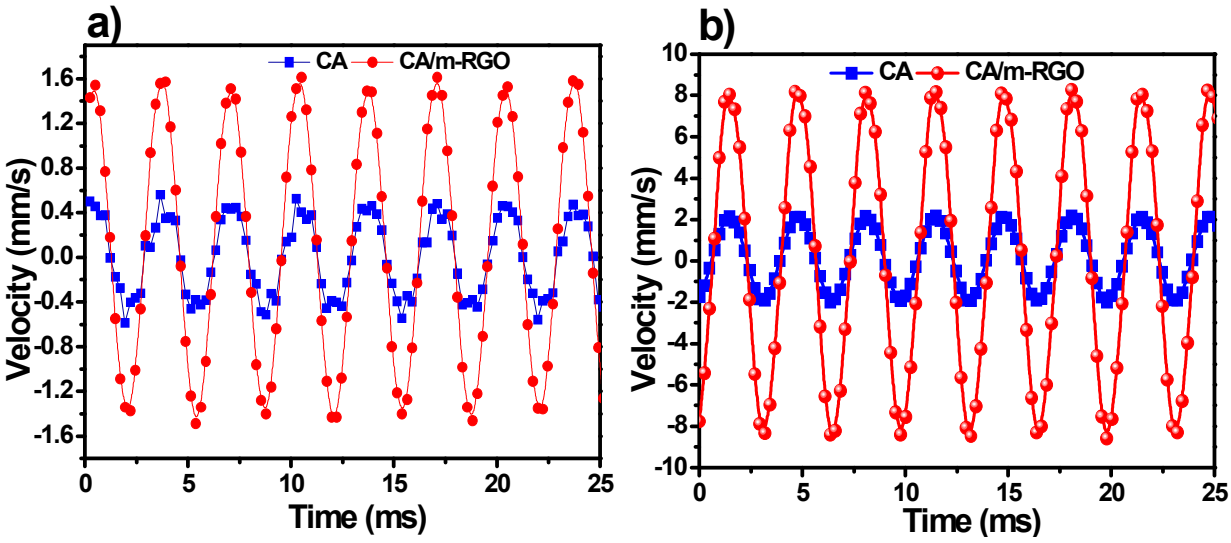

Figure 5. Tactile performance in terms of velocity change vs time at constant signal frequency 150 Hz and at voltage a) 200 V and b) 500V.

There are two main methods for utilizing the electrostatic force: using a change in the electrostatic force, or charging two electrode layers separated by a dielectric material.[5, 6, 19] The high dielectric constant of the composite also causes high electromechanical response. The results indicate that the self-assembled composite can generate a much higher strain as well as elastic energy density compared with neat polymer film. Such enhancement can be partly attributed to exchange coupling that is very effective when the size of second phase particles approaches nanometer scale and there are large electric field fluctuations in the polymeric matrix due to the large contrast of constituent dielectric constants.[1] The improvement in permittivity with nanoparticle loading and according to the experiments, the actuator performance is directly

influenced by the stiffness and dielectric constant of samples. Apparently, the stiffness increases with nanoparticle loading at a faster rate than the dielectric permittivity does. Relative permittivity of CA/m-RGO composite film is twofold larger than the pure CA film which indicates that superior charge storing capacity in composite film is the dominant factor to create the electrostatic force. Due to the intensified electrostatic attraction force between chargeable films performance is largely enhanced.

Frequency and voltage influence

Figure 6a shows the contour plot of the measured vibration velocity of the actuators at various applied frequencies from 25 to 225 Hz (at a fixed voltage of 500 V). Note that the vibration velocity was measured at the center of the film actuator. The vibration performance decreased close to the spacers and thus the points close to spacers provide a weaker tactile sensation in comparison to the center. It has also been reported that vibration at the low frequency range of 20–80 Hz is weakly felt by the finger, while vibration in the 150–250 Hz frequency range is most effective for information delivery through haptic feedback.[19] Figure 6b shows the responses of actuators of CA and CA/m-RGO composite films at 150 Hz with different voltage. Voltages ranging from 100 to 700 V were applied and vibration velocity was measured at the touch layer of the actuators. The vibration velocity of the CA/m-RGO composite film actuator exponentially increased with voltage whereas performance of CA film actuator increased linearly with applied voltage. Moreover, CA/m-RGO actuator was activated at low voltage while CA films actuator performance was around noise level at 100 V. At 700 V, the maximum vibration velocity of CA/m-RGO actuator reaches to 20 mm/s whereas it was around 4

mm/s for pure CA film samples. All the above performance measurement conditions clearly show the superior performance of CA/m-RGO actuator over pure CA film actuator.

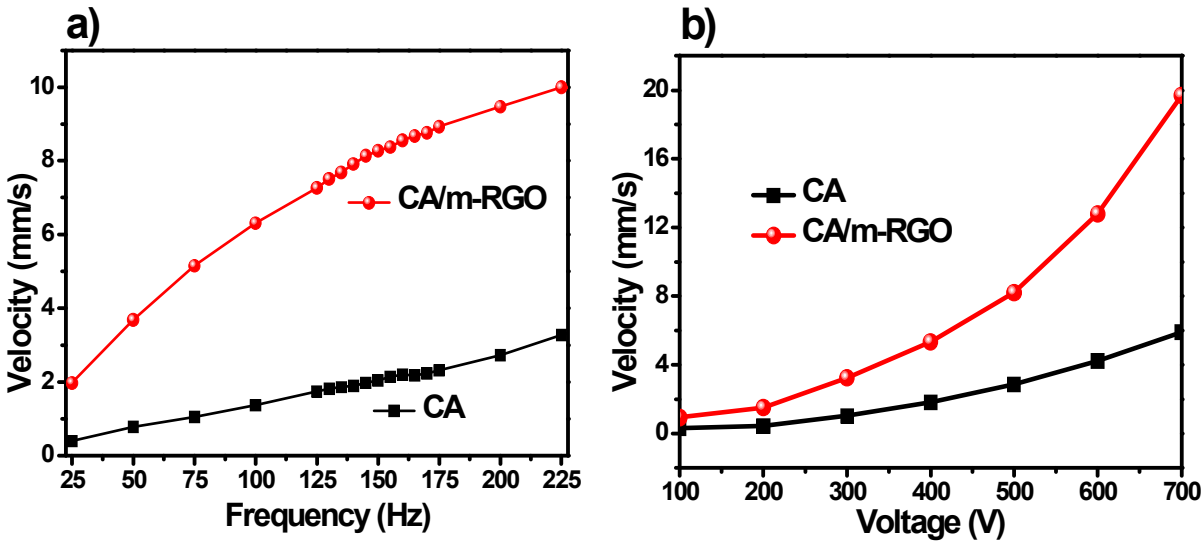

Figure 6. Velocity vs frequency at constant a) voltage 500V and b) signal frequency 150 Hz for CA and its composite film

Biased voltage

Figure 7 shows the bias voltage effect on the velocity of the CA/m-RGO actuator under a consistent sine wave signal of low level voltage at 150 Hz. With increasing the bias voltage, the output of the CA/m-RGO actuator increases. It suggests that bias voltage can be another important factor for further improvement of the actuator performance. Higher fixed charge loading with bias voltage can lead to denser surface charge, which produces higher electrostatic attraction force between electrodes of actuator. Moreover, biased voltage further reduced the activation voltage of CA/m-RGO actuator to 50 V.

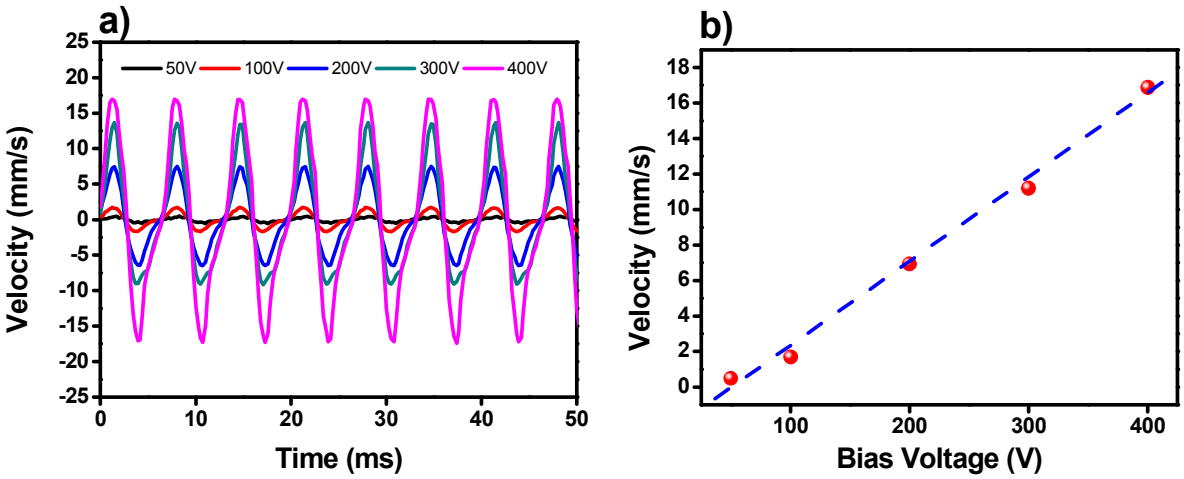

Figure 7. Bias voltage effect on CA/m-RGO actuation performance a) Velocity vs time and b) Velocity vs bias voltage plots

Temperature influence

The performance of actuators prepared by CA and CA/m-RGO composite films at 150 Hz applied frequency by varying the temperature is shown in Figure 8. As the temperature increases the performance curve of composite film actuator shows a steep decrease and fall around the level of pure CA film actuator, meanwhile, pure CA film actuator exhibit constant performance during the temperature range 25-60 ^{o}C. It may be given by the fact that the relaxation of chains, which are not in direct contact with filler surface is much more temperature-dependent than the retarded relaxation motion of chains in the inter phase region interacting directly with the filler surface. In other words, increasing temperature causes much faster softening of the bulk matrix in comparison with immobilized polymer chains (bound to the filler). Thus, increase of temperature of composite actuator film causes to rupture the weak physical polymer-filler bonds (chain desorption) arising at high strain amplitudes and results in decreased performance.[38]

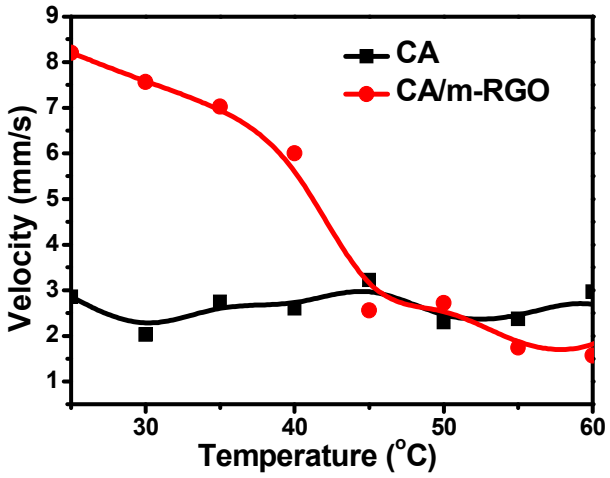

Figure 8. Temperature influence on tactile performance of CA and CA/m-RGO actuators.

Proof-of-concept for braille display

One way of solving the touch feeling issue is to create haptic actuators that can generate various button sensations via vibrotactile principle. There have been many studies to imitate button sensation using responsive actuators because tactile actuators can be easily designed in small dimension. A hardware prototype is presented that has been built to analyze the transmission characteristics of the braille board using actuation. The braille cell prototype was designed and fabricated using CA/graphene film as actuators. The proto type was used next to examine possible actuator efficiency in force-feedback control with designed actuator as shown in Figure 9.

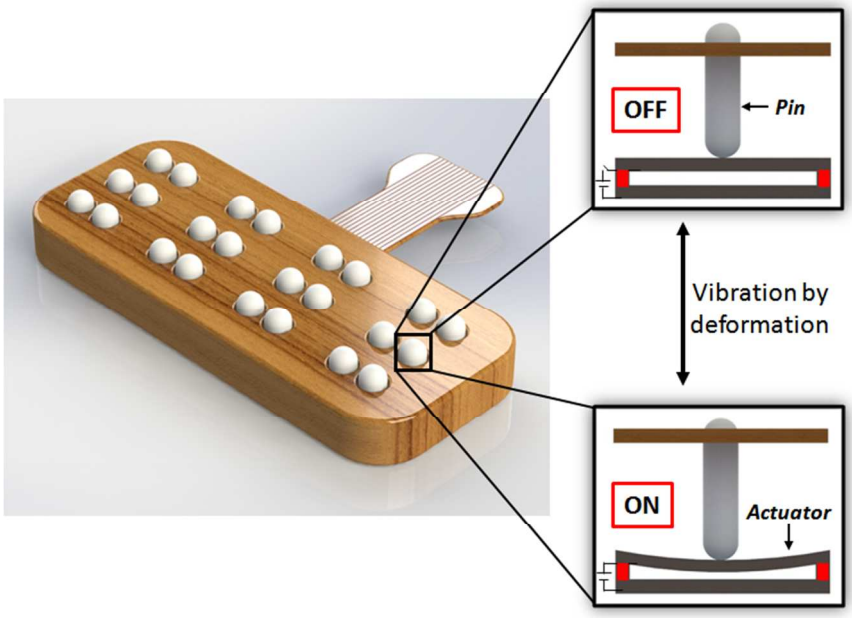

Figure 9. Schematic representation of braille cell using vibrotactile actuator.

The mimicking button sensation with vibration has a wide-frequency bandwidth (25–225 Hz) and the response time of the vibrotactile actuator will be smaller than the temporal resolution for haptic sensor (about 20 ms). Interestingly, it is worth noting that for now, flexible touch displays are used in curved and hard surfaces in which conventional tactile-feedback devices may be still useful. We observed the proposed vibrotactile actuator is small enough to be embedded in hand held devices, with fast response time, and creates vibrotactile force large enough to stimulate all mechanoreceptors. As shown in Figure S3, actuator performance has limitations depending on the type of wave function and sinusoidal form shows better performance than ramp and square type. Moreover, enhancement of mechanical properties also obtained with the presence of m-RGO (Figure S4). We also analyzed the repeatability of actuator by cyclic on and off voltage and found to have good reproducibility. The technology promises to bring new forms of tactile experience that will expand touch interaction with equipment and

make them feel more natural – while improving productivity, eco-friendliness and compatibility. The present advanced electronic devices adopting haptic technology rapidly spreads from a handful of consumer applications to a much more extensive scope of industrial, commercial, automotive, medical and different frameworks.

Conclusion

An actuator based on cellulose derived graphene composite was developed and applied for preferable execution of a braille tactile display. The proposed system exhibits controlled vibrotactile performance with respect to vibration amplitude, bias voltage and frequency. At the point when the film vibrator was working at its low voltage (50 V) and at frequency 150 Hz enough haptic sensation was observed around one μm of vibration amplitude. This device shows excellent actuator performance. However, its performance degrades with time and high temperature conditions. A proof-of-concept was explicated with lightweight, flexible, cheap, compact and expeditious time and furthermore gives touch-coordinate particular replication of braille display.

Acknowledgment

This work was supported by National Research Foundation (NRF-2013M3C1A3059586), Republic of Korea.

References

1. M. Mohiuddin, H.-C. Kim, S. Y. Kim and J. Kim, *Proc. of SPIE*, 2014, **9060**, 906017-1 to 4.
2. L. Thurfjell, J. McLaughlin, J. Mattsson and P. Lammertse, *Ind. Robot.*, 2002, **29**, 210-215.
3. S. D. Laycock and A. M. Day, *Comput. Graph. Forum*, 2003, **22**, 117-32.
4. K. J. Kuchenbecker, J. Fiene and G. Niemeyer, *IEEE T. Vis. Comput. Gr.*, 2006, **12**, 219-230.

5. O. Bau, I. Poupyrev, A. Israr and C. Harrison, *Proc. of the 23nd annual ACM symp. On UIST*, 2010, **UIST'10**, 283-292.
6. M.-C. Choi, Y. Kim and C.-S. Ha, *Prog. Polym. Sci.*, 2008, **33**, 581–630.
7. A. N. Sokolov, B. C.-K. Tee, C. J. Bettinger, J. B.-H. Tok and Z. Bao, *Acc. Chem. Res.*, 2011, **45**, 361-71.
8. T. Someya , Y. Kato, T. Sekitani, S. Iba, Y. Noguchi, Y. Murase, H. Kawaguchi and T. Sakurai, *Proc. Natl. Acad. Sci.*, 2005, **102**, 12321- 12325.
9. G. Kovacs and L. During, *Proc. SPIE*, 2009, **7287**, 72870A-1 to 15.
10. Y. Hui-Jian, Y. Li, S. Wen-Zhu, S. Song-Bai and Z. Liang, *RSC Adv.*, 2013, **3**, 23730-23736.
11. F. Carpi, G. Frediani and D. D. Rossi, *Proc. SPIE*, 2010, **7642**, 76420E-1 to 6.
12. K. Ren, L. Sheng, L. Minren, W. Yong and Q.M. Zhang, *Sens and Actu A: Phys*, 2008, **143,** 335–342.
13. N. D. Spigna, P Chakraborti, D. Winick, P. Yang, T. Ghosh and P. Franzon, *Proc. SPIE*, 2010, **7642**, 76420A-1 to 9.
14. A. B. Dalton, S. Collins, J. Razal, E. Munoz, V. H. Ebron, B. G. Kim, J. N. Coleman, J. P. Ferraris and R. H. Baughman, *J. Mater. Chem.*, 2004, **14**, 1-3.
15. R. J. Wood, E. Steltz and R. S. Fearing, *Sensor Actuat. A-Phys.*, 2005, **119**, 476-488.
16. D.-H. Kim, B. Kim and H. Kang, *Microsyst. Technol.*, 2004, **10**, 275-280.
17. M. Wagner, A. Roosen, H. Oostra, R. Hoppener and M. D. Moya, *J. Electroceram.*, 2005, **14**, 231-238.
18. A. V. Bune, C. Zhu, S. Ducharme, L. M. Blinov, V. M. Fridkin, S. P. Palto, N. N. Petukhova and S. G. Yudin, *J. Appl. Phys.*, 1999, **85**, 7869–7873.
19. D. Ponnamma, K. K. Sadasivuni, M. Strankowski, Q. Guo and S. Thomas, *Soft Matter*, 2013, **9**, 10343-10353.
20. A. Ambrosy and K. Holdik, *J. Phys. E: Sci. Intrum.*, 1984, **17**, 856-9.
21. A. Kafy, K. K. Sadasivuni, H.-C. Kim, A. Akther and J. Kim, *Phys. Chem. Chem. Phys.*, 2014, DOI: 10.1039/C4CP05921B.
22. K. K. Sadasivuni, M. Yadav, X. Gao, S. Mun and J. Kim, *Proc. SPIE*, 2014, **9060**, 906016-1 to 6.

23. H. S. Barud, A. M. D. Araújo, D. B. Santos, R. M. N. D. Assunção, C. S. Meireles, D. A. Cerqueira, G. R. Filho, C. A. Ribeiro, Y. Messaddeq and S. J. L. Ribeiro, *Thermochim. Acta*, 2008, **471**, 61–69.
24. D.-G. Yu, J.-H. Yu, L. Chen, G. R. Williams and X. Wang, *Carbohydr. Polym.*, 2012, **90**, 1016–1023.
25. M. K. Shin, B. Lee, S. H. Kim, J. A. Lee, G. M. Spinks, S. Gambhir, G. G. Wallace, M. E. Kozlov, R. H. Baughman and S. J. Kim, *Nat. Commun.*, 2012, **3**, 650-1 to 8.
26. A. B. Dalton, S. Collins, E. Muñoz, J. M. Razal, V. H. Ebron, J. P. Ferraris, J. N. Coleman, B. G. Kim and R. H. Baughman, *Nature*, 2003, **423**, 703.
27. N. Lachman, C. Bartholome, P. Miaudet, M. Maugey, P. Poulin and H. D. Wagner, *J. Phys. Chem. C*, 2009, **113**, 4751–4754.
28. M. Gopiraman, K. Fujimori, K. Zeeshan, B. S. Kim and I. S. Kim, *Express Polymer Letters*, 2013, **7**, 554–563.
29. K. K. Sadasivuni, D. Ponnamma, J. Kim and S. Thomas, *Graphene-Based Polymer Nanocomposites in Electronics*, Springer publisher, Switzerland, 2015, p. 67.
30. K. K. Sadasivuni, D. Ponnamma, S. Thomas and Y. Grohens, *Prog. Polym. Sci.*, 2014, **39**, 749–780.
31. D. Ponnamma, K. K. Sadasivuni, M. Strankowski, P. Moldenaers, S. Thomas and Y. Grohens, *R. Soc. Chem. Adv.*, 2013, **3**, 16068-16079.
32. T. Yamada, Y. Hayamizu, Y. Yamamoto, Y. Yomogida, A. Izadi-Najafabadi, D. N. Futaba and K. Hata, *Nat. Nanotechnol.*, 2011, **6**, 296-301.
33. U. Kim, J. Kang, C. Lee, H. Y. Kwon, S. Hwang, H. Moon, J. C. Koo, J.-D. Nam, B. H. Hong, J.-B. Choi and H. R. Choi, *Nanotechnology*, 2013, **24**, 145501 (7pp).
34. K. K. Sadasivuni, A. Kafy, L. Zhai, H.-U. Ko, S. Mun and J. Kim, *Small*, 2014, DOI: 10.1002/smll.201402109.
35. N. O. Weiss, H. Zhou, L. Liao, Y. Liu, S. Jiang, Y. Huang and X. Duan, *Adv. Mater.*, 2012, **24**, 5782–5825.
36. X. Cao, D. Qi, S. Yin, J. Bu, F. Li, C. F. Goh, S. Zhang and X. Chen, *Adv. Mater.*, 2013, **25**, 2957–2962.
37. D. C. Marcano, D. V. Kosynkin, J. M. Berlin, A. Sinitskii, Z. Sun, A. Slesarev, L. B. Alemany, W. Lu and J. M. Tour, *ACS Nano*, 2010, **4**, 4806–14.

38. K. K. Sadasivuni, D. Ponnamma, B. Kumar, M. Strankowskie, R. Cardinaels, P. Moldenaers, S. Thomas and Y. Grohens, *Compos. Sci. Technol.*, 2014, **104**, 18–25.
39. S. Littlejohn, A. Nogaret, G. Prentice and G. Pantos, *Adv. Funct. Mater.*, 2013, **23**, 5398 - 5402.
40. S. Pang, Y. Hernandez, X. Feng, and K. Mullen, *Adv. Mater.*, 2011, **23**, 2779–2795.
41. J.-K. Yuan, S.-H. Yao, Z.-M. Dang, A. Sylvestre, M. Genestoux and J. Bai, *J. Phys. Chem. C*, 2011, **115**, 5515-5521.
42. K. K. Sadasivuni, M. Castro, A. Saiter, L. Delbreilh, J. F. Feller, S. Thomas and Y. Grohens, *Mater. Lett.*, 2013, **96**, 109–112.
43. V. Loryuenyong, K. Totepvimarn, P. Eimburanapravat, W. Boonchompoo, and A. Buasri, *Adv. Mater. Sci. Eng.*, 2013, DOI: 10.1155/2013/923403.